ELSEVIER

Applied Ocean Research 23 (2001) 125–137

Applied Ocean Research

www.elsevier.com/locate/apor

Estimates of wave decay rates in the presence of turbulent currents

L. Thais[a,*], G. Chapalain[b], G. Klopman[c], R.R. Simons[d], G.P. Thomas[e]

[a]*Laboratoire de Mécanique de Lille, Université des Sciences et Technologies de Lille, URA-CNRS 1441, 59655 Villeneuve d'Ascq Cedex, France*
[b]*Université des Sciences et Technologies de Lille, Sédimentologie et Géodynamique, UMR-CNRS 8577, 59655 Villeneuve d'Ascq Cedex, France*
[c]*Albatros Flow Research, P.O. Box 85, 8325 ZH Vollenhove, The Netherlands*
[d]*Civil and Environmental Engineering, University College London, Gower Street, London WC1E 6BT, UK*
[e]*Department of Mathematical Physics, University College, Cork, Ireland*

Received 23 October 2000; revised 11 April 2001

Abstract

A full-depth numerical model solving the free surface flow induced by linear water waves propagating with collinear vertically sheared turbulent currents is presented. The model is used to estimate the wave amplitude decay rate in combined wave current flows. The decay rates are compared with data collected in wave flumes by Kemp and Simons [J Fluid Mech, 116 (1982) 227; 130 (1983) 73] and Mathisen and Madsen [J Geophys Res, 101 (C7) (1996) 16,533]. We confirm the main experimental finding of Kemp and Simons that waves propagating downstream are less damped, and waves propagating upstream significantly more damped than waves on fluid at rest. A satisfactory quantitative agreement is found for the decay rates of waves propagating upstream, whereas not more than a qualitative agreement has been observed for waves propagating downstream. Finally, some wave decay rates in the presence of favourable and adverse currents are provided in typical field conditions.

Keywords: Water waves; Currents; Wave damping; Turbulence; Free surface

1. Introduction

Combined flows of water waves and slowly varying currents being the predominant hydrodynamic characteristics of coastal areas have prompted a large amount of work to testify the major review articles by Peregrine [19], Jonsson [8], and more recently by Thomas and Klopman [28]. These reviews were mainly concerned with the kinematics, rather than the dynamics, of wave current flows, which reflects the fact that viscous effects in wave current flows have been largely disregarded in the literature. It must be acknowledged that many important phenomena, such as wave refraction by currents, are explained within the frame of inviscid theories. Inviscid models are also known to provide good estimates for the wavelength in the presence of currents and to give accurate predictions of the wave-induced velocities far from boundaries [5,27].

However, fluid-friction effects play a significant role near the boundaries of wave current flows. The development of bed forms and sediment movement in coastal regions are generally ascribed to turbulence generated at the seabed. Bed turbulence is also the main cause of non-breaking wave attenuation in shoaling depths. A useful approach to study near-bed turbulence generated by waves and currents has been to develop bottom boundary layer models (see the review in Ref. [23]). This type of approach has met large success in providing the wave friction factor f_w, usually defined as twice the squared ratio of the maximum friction velocity to the wave free-stream velocity, for combined wave current flows. The wave friction factor is indeed a parameter of central interest in wave-propagation models, and in more general circulation models of coastal waters. In contrast, boundary layer models actually do not solve the wave motion. Therefore, they cannot predict directly the wave amplitude attenuation rate, or alternatively the mean wave decay rate $s = \mathrm{d}A/\mathrm{d}x_1$, which is a measure of the wave amplitude decrease in the direction of wave propagation, x_1. This is somehow regrettable in terms of validation of these models since the experimentalist has direct access to the decay rate s with wave gauges. It is always possible to find a relation between the friction factor f_w and the decay rate s, yet this is a task involving a number of assumptions when waves are superposed with a vertically sheared current. For instance, one has to admit that separated energy budgets for the waves and the current can be written. Furthermore, when using the wave action equation to arrive

* Corresponding author. Fax: +33-328767301.
E-mail address: laurent.thais@univ-lille1.fr (L. Thais).

0141-1187/01/$ - see front matter
PII: S0141-1187(01)00014-1

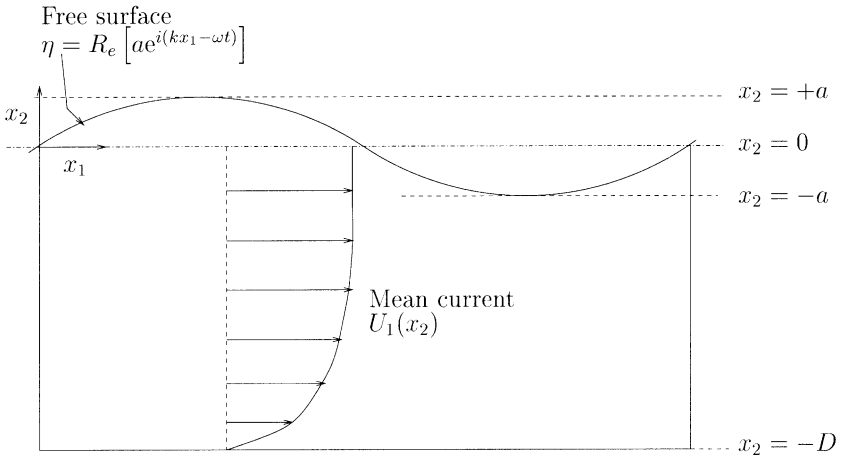

Fig. 1. Sketch of combined wave current flow with coordinate system used (here, waves propagating with a favourable current).

at s, a velocity scale representative of the sheared current must be chosen, and this is usually taken as the depth-averaged current without further justification (see Refs. [16–18,22]).

This paper presents a full-depth numerical model for the combined flow of regular waves and turbulent shearing currents. Our main intent here is to compute directly the wave amplitude decay rate by solving the wave motion in the primitive pressure-velocity formulation. This avoids resorting to the energy budget outlined above. To achieve this goal the boundary layer approximation is abandoned and the complex-valued wave number is computed directly as the eigenvalue of the problem. The real part of the wave number provides the wavelength, the imaginary part accounts for the wave attenuation. This is to some extent a generalisation of full-depth inviscid models in which the wave number was real-valued [27]. To keep things as simple as possible, we shall restrict ourselves to first order in the wave steepness of small amplitude regular waves collinear with the current, i.e. waves propagating with or against the current. Full-depth models for viscous wave current flows have appeared in the last few years but remain few. Klopman [12] derived the flow equations to second order in wave steepness with a one-equation turbulence closure, whereas Madden et al. [15] have developed a similar model with a stream-function formulation. We complete these works by improving the turbulence closure and making careful comparisons with available laboratory data.

The paper is organised as follows. The model assumptions, field equations, and boundary conditions are presented in Section 2. The numerical solution of the boundary value problem is outlined in Section 3. In Section 4, the present model predictions for the flow kinematics are qualitatively compared with Klopman's data [13]. In Section 5, wave decay rates are then quantitatively compared with Kemp and Simons' [10,11] and Mathisen and Madsen's [17] laboratory measurements. Generic results for wavelengths and wave attenuation rates in field conditions are also given in this section. Finally, the results are discussed and conclusions are given in Section 6.

2. Model formulation

2.1. Basic notations and assumptions

We consider a regular wave with amplitude a, absolute wave period T (as seen by a stationary observer), and wave number k travelling in the positive horizontal direction x_1 on water of constant finite depth D (see sketch in Fig. 1). The coordinate system (x_1, x_2) denotes the directions parallel and normal to the horizontal flat bottom, respectively, where x_2 is counted negative downwards between the mean water level $x_2 = 0$ and the bottom $x_2 = -D$. The wave number $k = k_r + \mathrm{i}k_i$ is allowed to be complex-valued, with $\mathrm{i} = \sqrt{-1}$, whereas the absolute radian frequency, $\omega = 2\pi/T$, is imposed to be a real quantity, i.e. only the spatial wave decay is considered. This is relevant to forced progressive waves in a flume, or freely travelling swell in the field.

The wave frequency ω is supposed to be known and constant, whereas the wavelength and the attenuation rate are computed in the presence of a current, which means that k_r and k_i are unknowns of the problem. The wave steepness $a|k| \simeq ak_r$ is further assumed sufficiently small so that the free surface elevation with respect to the mean water level is a circular function of the form

$$\eta = R_\mathrm{e}[a\mathrm{e}^{\mathrm{i}(kx_1-\omega t)}], \tag{1}$$

where R_e stands for the real part of the bracketed expression and t is the time. The above equation implies that the wave amplitude $A(x_1)$ at position x_1 is exponentially damped according to

$$A(x_1) = a\mathrm{e}^{-k_i x_1}, \qquad x_1 \geq 0, \tag{2}$$

where it can be seen that a is actually the wave amplitude taken at the origin $x_1 = 0$.

The velocity components are denoted by (U_1, U_2) in the

respective horizontal and vertical directions (x_1, x_2). The wave propagates with, or against, a vertically sheared horizontally uniform collinear current $U_1(x_2)$ (Fig. 1). This profile is clearly an approximation since a pumped current in a channel necessarily induces a mean surface slope, i.e. the depth of the flow must change and there must be an x_1 dependence of U_1, together with secondary circulations to satisfy continuity. We adopt a general hypothesis that the horizontal length scale over which U_1 varies is much longer than the wavelength, which means that we stay within the frame of a local analysis description.

The pressure is denoted by P. In most situations, turbulence will be generated near the flat bed. The turbulent kinetic energy is denoted by K and its dissipation rate by ϵ.

2.2. Phase-averaged equations

The turbulent wave current flow field has three components: a mean time-independent current, a periodic organized wave contribution, and random turbulent fluctuations. The phase-averaging operator $\langle F\rangle = (1/N)\sum_{k=0}^{N-1} F(t + kT)$, applied to any flow variable F and repeated over N regular waves with period T, filters the turbulent fluctuations from the mean and wavy flow fields (see Refs. [20] or [26] for details). This operator produces phase-averaged Reynolds equations from which the present model is derived

$$\frac{\partial\langle U_j\rangle}{\partial x_j} = 0, \tag{3}$$

$$\frac{\partial\langle U_i\rangle}{\partial t} + \langle U_j\rangle\frac{\partial\langle U_i\rangle}{\partial x_j} = -\frac{1}{\rho}\frac{\partial\langle P\rangle}{\partial x_i} + \frac{\partial\langle\tau_{ij}\rangle}{\partial x_j} + \nu\frac{\partial^2\langle U_i\rangle}{\partial x_j\partial x_j}. \tag{4}$$

We take $1 \le i, j \le 2$ and Einstein's summation applies over the repeated index j. In these equations, ν is the kinematic viscosity of water, ρ its density, and $\langle\tau_{ij}\rangle$ is the shear-stress components which are determined from the phase-averaged strain rate tensor according to the Boussinesq hypothesis

$$\langle\tau_{ij}\rangle = \langle\nu_t\rangle\left[\frac{\partial\langle U_i\rangle}{\partial x_j} + \frac{\partial\langle U_j\rangle}{\partial x_i}\right]. \tag{5}$$

The eddy viscosity $\langle\nu_t\rangle$ will be evaluated with Chien's low-Reynolds number 'K–ϵ' turbulence model [3]. The turbulence regime in the field is usually fully rough, yet laboratory measurements can span the whole range from smooth laminar to rough turbulent. Chien's model is able to predict unsteady flows in the vicinity of smooth, transitional and rough beds [24]. A better prediction of turbulence close to the bed is also expected in a low-Reynolds number formulation because of flow reversal within the wave boundary layer. Chien's transport equations for the turbulent moments are

$$\frac{\partial\langle K\rangle}{\partial t} + \langle U_j\rangle\frac{\partial\langle K\rangle}{\partial x_j} = \frac{\partial}{\partial x_i}\left[\left(\nu + \frac{\langle\nu_t\rangle}{\sigma_K}\right)\frac{\partial\langle K\rangle}{\partial x_i}\right] + \langle\tau_{ij}\rangle\frac{\partial\langle U_i\rangle}{\partial x_j} - 2\nu\frac{\langle K\rangle}{x_2^2} - \langle\epsilon\rangle, \tag{6}$$

$$\frac{\partial\langle\epsilon\rangle}{\partial t} + \langle U_j\rangle\frac{\partial\langle\epsilon\rangle}{\partial x_j} = \frac{\partial}{\partial x_i}\left[\left(\nu + \frac{\langle\nu_t\rangle}{\sigma_E}\right)\frac{\partial\langle\epsilon\rangle}{\partial x_i}\right] + C_{\epsilon1}\frac{\langle K\rangle}{\langle\epsilon\rangle}\langle\tau_{ij}\rangle\frac{\partial\langle U_i\rangle}{\partial x_j} + f_3\left(\frac{2\nu}{x_2^2}\right)\langle\epsilon\rangle - C_{\epsilon2}f_2\frac{\langle\epsilon\rangle^2}{\langle K\rangle}. \tag{7}$$

The phase-averaged eddy viscosity following from this pair of transport equations is

$$\langle\nu_t\rangle = C_\mu f_\mu\frac{\langle K\rangle^2}{\langle\epsilon\rangle}. \tag{8}$$

The damping functions appearing in the above equations are

$$f_\mu = 1 - \exp(-0.0115x_{2+}), \tag{9}$$

$$f_2 = 1 - \frac{2}{9}\exp[-(R_T/6)^2], \tag{10}$$

$$f_3 = \exp[-(x_{2+}/2)] \tag{11}$$

and the model constants take the values

$$(C_\mu, C_{\epsilon1}, C_{\epsilon2}, \sigma_K, \sigma_E) = (0.09, 1.35, 1.8, 1.0, 1.3). \tag{12}$$

The dimensionless number $R_T = \langle K\rangle^2/\nu\langle\epsilon\rangle$ of the damping function f_2 is a local turbulence Reynolds number, and $x_{2+} = (D + x_2)\langle u_\tau\rangle/\nu$ is a wall coordinate, with origin at the bed, scaled with the friction velocity $\langle u_\tau\rangle = \sqrt{|\langle\tau_{12}\rangle|/\rho}$. The eddy viscosity is not damped in the vicinity of the free surface in the absence of any better information. The near-surface decrease of $\langle\nu_t\rangle$ will be enforced via the surface boundary conditions for $\langle K\rangle$ and $\langle\epsilon\rangle$ (see Section 2.4).

2.3. Wave-like equations

Any phase-averaged flow variable $\langle F\rangle$ is split into a time-independent zero-order mean contribution F and a wave-like first-order contribution $\tilde{f}$ according to the expansion

$$\langle F\rangle(x_1, x_2, t) = F(x_2) + \tilde{f}(x_2)e^{i(kx_1 - \omega t)}, \tag{13}$$

where $\tilde{f}$ is a complex-valued wave-like amplitude, having zero mean, that represents the wave motion. The wave-like equations are obtained upon substituting Eq. (13) in the phase-averaged equations, and retaining the first-order terms (terms linear in $\tilde{f}$), the main mathematical benefit of the substitution being to transform partial differential equations in a system of linear ordinary differential equations in the independent variable x_2. This is a lengthy, yet straightforward process, and we therefore state the results

directly without further development. It should be added that the approximation $U_1 = U_1(x_2)$ is consistent with neglecting the vertical current U_2 in the following equations.

The wave-like continuity equation is

$$\mathrm{i}k\tilde{u}_1 + \frac{\mathrm{d}\tilde{u}_2}{\mathrm{d}x_2} = 0. \tag{14}$$

The wave-like momentum equations in directions x_1 and x_2 can be written in the convenient form

$$\mathrm{i}(kU_1 - \omega)\tilde{u}_1 + \frac{\mathrm{d}U_1}{\mathrm{d}x_2}\tilde{u}_2 + \mathrm{i}k\tilde{p} = (\nu + \nu_t)\left(\frac{\mathrm{d}^2\tilde{u}_1}{\mathrm{d}x_2^2} - k^2\tilde{u}_1\right) + \tilde{\alpha}\frac{\mathrm{d}\nu_t}{\mathrm{d}x_2} + \tilde{\nu}_t\frac{\mathrm{d}^2U_1}{\mathrm{d}x_2^2} + \frac{\mathrm{d}\tilde{\nu}_t}{\mathrm{d}x_2}\frac{\mathrm{d}U_1}{\mathrm{d}x_2}, \tag{15}$$

$$\mathrm{i}(kU_1 - \omega)\tilde{u}_2 + \frac{\mathrm{d}\tilde{p}}{\mathrm{d}x_2} = (\nu + \nu_t)\left(\frac{\mathrm{d}^2\tilde{u}_2}{\mathrm{d}x_2^2} - k^2\tilde{u}_2\right) + 2\frac{\mathrm{d}\nu_t}{\mathrm{d}x_2}\frac{\mathrm{d}\tilde{u}_2}{\mathrm{d}x_2} + \mathrm{i}k\tilde{\nu}_t\frac{\mathrm{d}U_1}{\mathrm{d}x_2}. \tag{16}$$

The conservation equations for the turbulent kinetic energy and its dissipation rate are

$$\mathrm{i}(kU_1 - \omega)\tilde{k} + \frac{\mathrm{d}K}{\mathrm{d}x_2}\tilde{u}_2 = \left(\nu + \frac{\nu_t}{\sigma_K}\right)\left(\frac{\mathrm{d}^2\tilde{k}}{\mathrm{d}x_2^2} - k^2\tilde{k}\right) + \frac{1}{\sigma_K}\left[\frac{\mathrm{d}\nu_t}{\mathrm{d}x_2}\frac{\mathrm{d}\tilde{k}}{\mathrm{d}x_2} + \tilde{\nu}_t\frac{\mathrm{d}^2K}{\mathrm{d}x_2^2} + \frac{\mathrm{d}\tilde{\nu}_t}{\mathrm{d}x_2}\frac{\mathrm{d}K}{\mathrm{d}x_2}\right] + 2\tilde{\alpha}\nu_t\frac{\mathrm{d}U_1}{\mathrm{d}x_2} + \tilde{\nu}_t\left(\frac{\mathrm{d}U_1}{\mathrm{d}x_2}\right)^2 - \left(\frac{2\nu}{z^2}\right)\tilde{k} - \tilde{\epsilon} \tag{17}$$

and

$$\mathrm{i}(kU_1 - \omega)\tilde{\epsilon} + \frac{\mathrm{d}\epsilon}{\mathrm{d}x_2}\tilde{u}_2 = \left(\nu + \frac{\nu_t}{\sigma_E}\right)\left(\frac{\mathrm{d}^2\tilde{\epsilon}}{\mathrm{d}x_2^2} - k^2\tilde{\epsilon}\right) + \frac{1}{\sigma_E}\left[\frac{\mathrm{d}\nu_t}{\mathrm{d}x_2}\frac{\mathrm{d}\tilde{\epsilon}}{\mathrm{d}x_2} + \tilde{\nu}_t\frac{\mathrm{d}^2\epsilon}{\mathrm{d}x_2^2} + \frac{\mathrm{d}\tilde{\nu}_t}{\mathrm{d}x_2}\frac{\mathrm{d}\epsilon}{\mathrm{d}x_2}\right] + C_{\epsilon 1}\frac{\epsilon}{K}\frac{\mathrm{d}U_1}{\mathrm{d}x_2}\nu_t\left(2\tilde{\alpha} + \frac{\mathrm{d}U_1}{\mathrm{d}x_2}\frac{\tilde{k}}{K}\right) - f_3\left(\frac{2\nu}{x_2^2}\right)\tilde{\epsilon} - C_{\epsilon 2}f_2\frac{\epsilon}{K}\left(2\tilde{\epsilon} - \frac{\epsilon}{K}\tilde{k}\right). \tag{18}$$

In Eqs. (15), (17) and (18) we have set

$$\tilde{\alpha} = \tilde{\alpha}(\tilde{u}_1, \tilde{u}_2) = \frac{\mathrm{d}\tilde{u}_1}{\mathrm{d}x_2} + \mathrm{i}k\tilde{u}_2. \tag{19}$$

The first-order eddy viscosity $\tilde{\nu}_t$ in the same equations arises from the linear expansion of Eq. (8), namely

$$\tilde{\nu}_t = \nu_t\left[2\left(\frac{\tilde{k}}{K}\right) - \frac{\tilde{\epsilon}}{\epsilon}\right]. \tag{20}$$

The present model is a wave model in the sense that it just predicts the modifications of the wave kinematics by a given current distribution; it is not aimed at predicting the zero-order terms appearing in the wave-like equations.[1] This means we do not attempt to predict changes of the current under wave action, we shall compute the wave motion as 'reaction' to a mean current altered by waves, and which must be considered as input to the wave model. Therefore, the zero-order terms in the wave-like equations need to be specified before seeking a solution for the wave-like amplitudes. Mean currents in the presence of waves can be specified from measurements, if available, computed with boundary layer type models, or computed with 'generative' wave current models as recently developed by Groeneweg and Klopman [6]. For the purpose of the present work they have been evaluated with a numerical boundary layer wave current model [25]; details about the numerical model for waves with no current can also be found in Ref. [24]. This numerical boundary layer model is built on the same ground as the model of Davies et al. [4] but includes Chien's turbulence closure. Boundary layer type models can predict the slowing down of the mean current in the bed region due to wave mixing, but are known to behave poorly in the near-surface region. Turbulent sheared currents in the presence of waves are the object of another study under way and will not be considered within this paper which is focused on the wave motion.

2.4. Boundary conditions

2.4.1. Phase-averaged boundary conditions

The bottom boundary conditions are naturally imposed at the bed level. They specify impermeability of the bed and equilibrium conditions for the turbulent moments

$$\langle U_1\rangle = \langle U_2\rangle = 0, \tag{21}$$

$$\langle K\rangle = \langle u_\mathrm{f}\rangle^2\beta(R_k), \tag{22}$$

$$\langle\epsilon\rangle = \frac{C_\mu^{3/4}\langle K\rangle^{3/2}}{\kappa z_0}, \qquad x_2 = -D, \tag{23}$$

where $\kappa = 0.4$ is the Kàrmàn constant. The bed has a roughness length z_0 and an equivalent sand roughness height $k_\mathrm{s} = 30z_0$. The bottom boundary conditions for the turbulent moments depend upon the roughness Reynolds number $R_k = \langle u_\mathrm{f}\rangle k_\mathrm{s}/\nu$ through the function

$$\beta(R_k) = \frac{C_\mu^{1/2}}{\kappa^2}\left[\frac{30}{R_k} + \left(\frac{900}{R_k^2} + \frac{C_\mu}{\kappa^2}\right)^{1/2}\right]^{-2}. \tag{24}$$

[1] This is a 'reactive' wave current model in the parlance of Thomas and Klopman [28].

These expressions are valid for smooth, transitional and rough boundaries [24].

The free surface boundary conditions raise two kinds of complications. The first difficulty is due to the oscillatory nature of the free surface whereas we need to apply the boundary conditions on a flat coordinate line. This will be addressed with a Taylor series expansion in Section 2.4.2. The second, and major, difficulty comes from the little knowledge that we have of the turbulence behaviour near a free surface. Eddies near a free surface are known to be damped, inducing higher dissipation than in a free stream. The practical implication for models is that turbulent closure schemes must reflect the decrease in the eddy viscosity (or equivalently in the turbulent length scale) in the near-surface region. Full symmetry conditions, i.e. $\mathrm{d}\langle K\rangle/\mathrm{d}x_2 = \mathrm{d}\langle\epsilon\rangle/\mathrm{d}x_2 = 0$, lead to eddy viscosity profiles erroneously increasing towards the surface. This is in contradiction with measurements in channel flows. To take this into account we have adopted the scheme proposed by Celik and Rodi [2], which consists of imposing the level of dissipation rate at the free surface.

To summarise, in the absence of wind traction and surface tension effects being neglected, the upper boundary conditions applied on the surface level $x_2 = \eta(x_1, t)$, are

$$\langle\tau_{12}\rangle = 0, \tag{25}$$

$$\langle\tau_{22}\rangle = \langle P\rangle, \tag{26}$$

$$\frac{\mathrm{d}\langle K\rangle}{\mathrm{d}x_2} = 0, \tag{27}$$

$$\langle\epsilon\rangle = \frac{\gamma\langle K\rangle^{3/2}}{D}, \qquad x_2 = \eta(x_1, t). \tag{28}$$

Following Celik and Rodi [2] we take $\gamma = 5.87$ in the empirical expression (28).

2.4.2. Wave-like boundary conditions

Similarly to the field equations, the wave-like bottom boundary conditions are derived from the first-order expansion of the phase-averaged expressions. We get straightforwardly

$$\tilde{u}_1 = \tilde{u}_2 = 0, \tag{29}$$

$$\tilde{k} = \frac{\tilde{\tau}_\mathrm{b}}{\rho}\beta(R_k), \tag{30}$$

$$\tilde{\epsilon} = \frac{3}{2}\left(\frac{C_\mu^{3/4}K^{1/2}}{\kappa z_0}\right)\tilde{k}, \qquad x_2 = -D, \tag{31}$$

where $\tilde{\tau}_\mathrm{b}/\rho$ is the first-order tangential stress

$$\frac{\tilde{\tau}_{12}}{\rho} = (\nu + \nu_t)\tilde{\alpha}(\tilde{u}_1, \tilde{u}_2) + \tilde{\nu}_t\frac{\mathrm{d}U_1}{\mathrm{d}x_2} \tag{32}$$

evaluated at the bed level; $\tilde{\alpha}(\tilde{u}_1, \tilde{u}_2)$ was defined in Eq. (19).

The wave-like surface boundary conditions are obtained with a two-step procedure. The phase-averaged expressions (25)–(28) for any quantity $\langle F\rangle$ are projected onto the mean surface level $x_2 = 0$ according to the Taylor series

$$\langle F\rangle_{x_2=\eta} = \langle F\rangle_{x_2=0} + a\left(\frac{\mathrm{d}\langle F\rangle}{\mathrm{d}x_2}\right)_{x_2=0} \tag{33}$$

and the first-order terms are then retained from these expressions. For the tangential stress this reads

$$\frac{\tilde{\tau}_{12}}{\rho} = -a\left[(\nu + \nu_t)\frac{d^2U_1}{\mathrm{d}x_2^2} + \frac{\mathrm{d}\nu_t}{\mathrm{d}x_2}\frac{\mathrm{d}U_1}{\mathrm{d}x_2}\right], \qquad x_2 = 0. \tag{34}$$

For the normal stress we arrive at a balance involving the wave-like pressure field and the acceleration of gravity g, namely

$$\tilde{p} = 2(\nu + \nu_t)\frac{\mathrm{d}\tilde{u}_2}{\mathrm{d}x_2} + ag, \qquad x_2 = 0. \tag{35}$$

The turbulent kinetic energy and the dissipation rate are constrained by

$$\frac{\mathrm{d}\tilde{k}}{\mathrm{d}x_2} + a\frac{\mathrm{d}^2K}{\mathrm{d}x_2^2} = 0, \tag{36}$$

$$\tilde{\epsilon} + a\frac{\mathrm{d}\epsilon}{\mathrm{d}x_2} = \frac{3}{2}\gamma\frac{\sqrt{K}}{D}\left(\tilde{k} + a\frac{\mathrm{d}K}{\mathrm{d}x_2}\right), \qquad x_2 = 0. \tag{37}$$

Finally, the kinematic surface condition, specific to the wave motion, expresses that the free surface is impermeable and moves vertically with velocity $\tilde{u}_2$, namely

$$\tilde{u}_2 = \mathrm{i}a(kU_1 - \omega), \qquad x_2 = 0. \tag{38}$$

3. Numerical solution for the wave-like amplitudes

At the first stage of the model the zero-order variables of the mean current motion, as well as their first and second derivatives with respect to x_2, are evaluated with a cubic spline interpolation on the grid of the wave problem. Once this is done, a solution can be sought for the wave-like amplitudes.

Eq. (14)–(18) form a set of nine first-order linear ordinary differential equations (ODEs) of the boundary value type for the complex-valued variables $\tilde{p}$, $\tilde{u}_1$, $\tilde{u}_2$, $\tilde{k}$, $\tilde{\epsilon}$ together with the first derivative with respect to x_2 of the last 4 of these. The set of ODEs is solved with the double precision built-in routine DBVPFD of the mathematical package IMSL. The algorithm is based upon a second order accurate finite difference relaxation method.

The main difficulty here is to find the eigenvalue of the problem, namely the wave number k, and especially the imaginary wave number which is commonly three orders of magnitude smaller than the real wave number. We found it numerically efficient to treat k as an additional dependent variable constant over depth, i.e. satisfying the differential equation $\mathrm{d}k/\mathrm{d}x_2 = 0$, which was added to the nine original

ODEs. The final set of ten first-order ODEs is closed when subject to an equal number of boundary conditions. Eqs. (29)–(31) together with Eqs. (34)–(38) provide all of them but one. To close the system the mass conservation Eq. (14) was enforced at the free surface level, since only its first derivative is actually used when evaluating the function derivatives and the Jacobian. In the same time, this choice avoids computing a velocity field arbitrarily shifted by a constant from the true physical solution.

The finite difference grid used to solve the problem is adaptive with logarithmic refinements near the surface and bottom. Initial guesses for the unknowns are provided by inviscid linear wave theory.

Klopman et al. [14] present a detailed inter-comparison study where the consistency of the present model, particularly in terms of accuracy of the computed real and imaginary wave numbers, has been tested against analytical solutions and other numerical models. The present numerical algorithm is fast, self-consistent and accurate. Computational efforts are as small as a couple of seconds on a basic workstation for a standard grid having 2000 mesh points.

4. Comparison of flow kinematics

Before moving on to the wave decay rate, which is the main topic of this study, we shall examine the predictive ability of the present model in terms of flow kinematics over the full water depth. Klopman [13] made extensive measurements of combined wave current flows in a wave flume at Delft Hydraulics. He has provided a very detailed description of wave current flows measured over the entire water column with a laser velocimeter.

The results for Klopman's experiment labelled DHFC01 will be considered here. The flow conditions were $D = 0.5$ m, with a depth-averaged favourable current $\bar{U}_1 = 0.152$ m/s flowing with regular waves having a period $T = 1.44$ s and an amplitude $a = 0.06$ m. The concrete bed of the test flume was roughened with pasted natural coarse sand. This produced an equivalent sand roughness $k_s = 1.2$ mm leading to transitional turbulent conditions (peak roughness Reynolds number of order 10).

Fig. 2a displays the amplitude of the horizontal velocity $\tilde{u}_1$ as a function of depth. Fig. 2b is a close-up view of the wave boundary layer region. Two curves are plotted in Fig. 2b to look more carefully at the boundary layer structure. The solid curve is the result of the turbulent numerical model which includes the eddy viscosity evaluated with the Chien model. The dashed curve is the result of a laminar model that accounts for molecular viscosity alone, i.e. setting $\langle \nu_t \rangle = 0$ in the momentum equations and omitting the turbulent moment equations. In both instances the molecular viscosity was $\nu = 1.13 \times 10^{-6}$ m^2/s. Not surprisingly, the solid curve is a better fit to the data. The laminar solution predicts a boundary layer extent that is clearly too narrow. Madden et al. [15] have also shown on the same data set that an eddy viscosity based upon the current alone, i.e. neglecting $\tilde{\nu}_t$ but retaining ν_t, does not work very well either. The present model, which does include $\tilde{\nu}_t$, improves slightly the near-bed solution but it remains that our predictions still suffer a deficiency in the magnitude of the velocity overshoot. Wave reflection in the tank and non-linear interactions, not accounted for in the model, are possible explanations to the remaining discrepancy. Considering that the difference between the measurements and the computed profile remains within the experimental error bar (of order 0.01 m/s for this particular dataset), it seems that the present model gives an acceptable description of the flow kinematics over the entire water depth.

Fig. 2a and b are also a meaningful illustration of the usefulness of the present full-depth model. Any boundary layer model would be typically able to predict this flow in the near-bed region. Predicting the flow up to the free surface with a boundary layer model would then require a matching with an inviscid theory, thereby raising other difficult questions: Which wave theory should be used? What is the optimal height to apply the matching? What is the value of the wavelength? The present full-depth approach circumvents the above mentioned difficulties and predicts directly the amplitude decay rate.

5. Wave decay rates in the presence of currents

5.1. Mean wave decay rate

From the experimental results available [1,10,11,17] the wave amplitude decay rate in the presence of currents seems to remain exponential, as it is for waves alone in a channel [7]. This implies Eq. (2) does seem relevant to wave current flows. However, experimental results have often been presented in terms of a mean amplitude decay rate $s = \mathrm{d}A/\mathrm{d}x_1$ [10,11,17]. This amounts to a straight-line fit through the experimental points over a distance L covered by wave gauges, instead of fitting an exponential curve. For the sake of clarity we shall stick to this approach. Therefore, the experimental wave decay rates will be compared with the computed decay rates s_c averaged from Eq. (2) over the distance L, namely

$$s_c = \frac{a}{L}(\mathrm{e}^{-k_i L} - 1), \tag{39}$$

where it is recalled that the imaginary wave number k_i is directly output by the numerical model. For $k_i L = \mathrm{o}(1)$, Eq. (39) reduces to $s_c = -ak_i$.

The model predictions coming from Eq. (39) still cannot be compared with the raw experimental decay rates s_e since, in a channel, the side-walls account for part of the attenuation. Following Hunt [7], Simons et al. [22], and Mathisen and Madsen [17] the side-wall decay rate will be evaluated

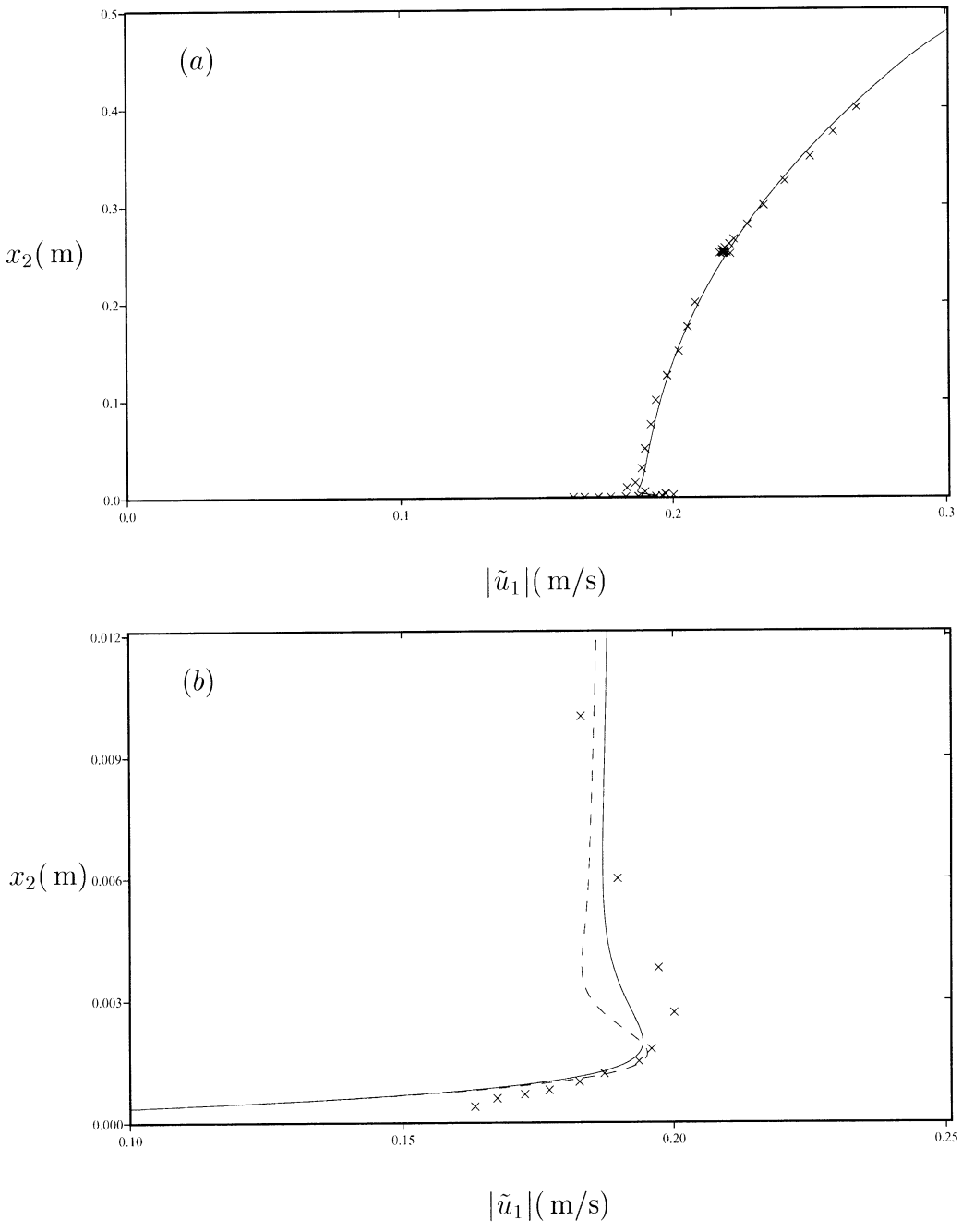

Fig. 2. Wave-like horizontal velocity amplitude in Ref. [13] DHFC01 experiment: (a) full-depth view, (b) close-up view of the bottom 1.2 cm; —, model prediction with Chien turbulence closure, - - -, model prediction for laminar flow ($\nu = 1.13 \times 10^{-6}$ m^2/s, $\nu_t = \tilde{\nu}_t = 0$); +, experimental points.

with

$$s_{es} = -\sqrt{\frac{\nu}{2\omega}}\frac{a_m \omega}{B c_g}. \tag{40}$$

Here, c_g is the group velocity of small amplitude regular waves (see e.g. Ref. [16]), and B is the channel breadth, and

$$a_m = a\left(\frac{\sinh 2k_r D}{Bk_r + \sinh 2k_r D}\right) \tag{41}$$

is an amplitude representative of the wave motion. Eq. (40) accounts only for purely viscous effects. It has been derived for waves alone, and Simons et al. [22] have raised doubts about its use for combined waves and currents. The wave energy dissipation rates at the bed and the sidewalls are linear functions of the wave amplitude. Therefore, the experimental wave decay rates related to bottom friction presented further down, and noted s_{eb}, have been evaluated from the raw measured decay rates s_e through the difference [17]

$$s_{eb} = s_e - s_{es}. \tag{42}$$

5.2. Comparison with laboratory data

5.2.1. Kemp and Simons' data

Detailed measurements of the flow kinematics and dynamics of waves in the presence of collinear favourable and opposing currents were carried out by Kemp and Simons [10,11]. They worked with linear 1s-waves in water depth of 20 cm over both a smooth plate and an artificially roughened bed. Their test flume was 0.457 m wide and had side-walls of smooth plate-glass. Their main finding regarding wave attenuation was that, with respect to waves alone, the wave decay rate was greatly increased for waves propagating against the current, and moderately decreased for waves propagating with the current. This appeared to hold for smooth and rough beds. For the opposing current this finding corroborates a comment by Yih [29] who had pointed out earlier that waves propagating upstream may become damped out.

Fig. 3 depicts the raw measured wave decay rates, their values corrected for side-wall effects, and the computed decay rates. In Table 1, Kemp and Simons' [10,11] measured decay rates and the corresponding computed values have been collected to make the interpretation easier. In this table, we have distinguished between the raw experimental values s_e, the side-wall contribution s_{es} evaluated with Eq. (40), and the resulting bed contribution issued from Eq. (42). The two right-most columns in this table should be compared. The sidewall wave decay rate contributes in-between 5 and 10% of the raw measured values.

Considering the four waves alone reference experiments WR1 through WR5, there is a tendency of the model to under-predict the wave decay rate in proportion of around 15–20%. The agreement is better for the WDR adverse current experiments (except WDR5 which had the steepest wave), the model predicting successfully a significant increase in the wave decay rate with increasing wave amplitude. The favourable current cases (experiments WCR) exhibit somewhat less satisfactory results. The tendency of the model is again to under-predict the wave decay rate, yet the relative decrease in wave damping with respect to waves alone is at least qualitatively reproduced.

5.2.2. Mathisen and Madsen's data

Mathisen and Madsen [17] have only considered waves on a favourable current. These authors worked in a rough bed wave flume, in water depth of 60 cm with waves 2.2, 2.6, and 2.9 s in period. Here, the flume breadth was $B = 0.76$ m and the sidewalls were made of smooth glass. They published wave decay rates corrected for sidewall effects in the same way as in Eq. (42). Table 2 compiles the results for 10 of their experiments which we have computed. The wave current values are displayed in Fig. 4.

Mathisen and Madsen find the same qualitative behaviour as in Kemp and Simons' experiments, namely the wave decay rates in the presence of favourable currents are smaller than on fluid at rest. However, the decrease in the decay rates with respect to waves alone is markedly less than in the Kemp and Simons' study.

In the three waves alone experiments our predicted wave decay rates are on average 30% smaller than the estimated experimental values. When looking at the wave current experiments one sees that the model prediction is also on average 30% less than the wave decay rates estimated from the data for values of the wave current strength ζ less than unity. The best agreement between the model results and the experimental data is found at large values of ζ. Yet, the marked increase in the experimental decay rates at the highest wave current strengths seems rather difficult to understand, and the present model is certainly unable to predict this feature.

Table 1
Wave amplitude decay rates in the experiments of Refs. [10,11]

Experiment ID	Wave current strength $\zeta = a\omega/\bar{U}_1$	Exp. decay rate (total) $s_e \times 10^5$	Exp. decay rate (side-wall) $s_{es} \times 10^5$	Exp. decay rate (bed) $s_{eb} \times 10^5$	Computed decay rate $s_c \times 10^5$
Rough wall, waves alone					
WR1	∞	−41.0	−3.8	−37.2	−30.1
WR3	∞	−58.0	−5.0	−53.0	−38.4
WR4	∞	−69.0	−6.2	−62.8	−50.6
WR5	∞	−68.0	−6.6	−61.4	−50.7
Rough wall, adverse current					
WDR1	−0.8	−67.0	−3.8	−63.2	−51.0
WDR2	−0.9	−75.0	−4.6	−70.4	−62.1
WDR3	−1.1	−85.0	−5.4	−79.6	−75.1
WDR4	−1.4	−112.0	−6.9	−105.1	−98.4
WDR5	−1.7	−170.0	−8.1	−161.9	−117.6
Rough wall, favourable current					
WCR1	+0.4	−20.0	−3.1	−16.9	−11.5
WCR3	+0.5	−27.0	−4.3	−22.7	−12.9
WCR4	+0.7	−23.0	−5.6	−17.4	−14.3
WCR5	+0.8	−26.0	−6.4	−19.6	−15.1

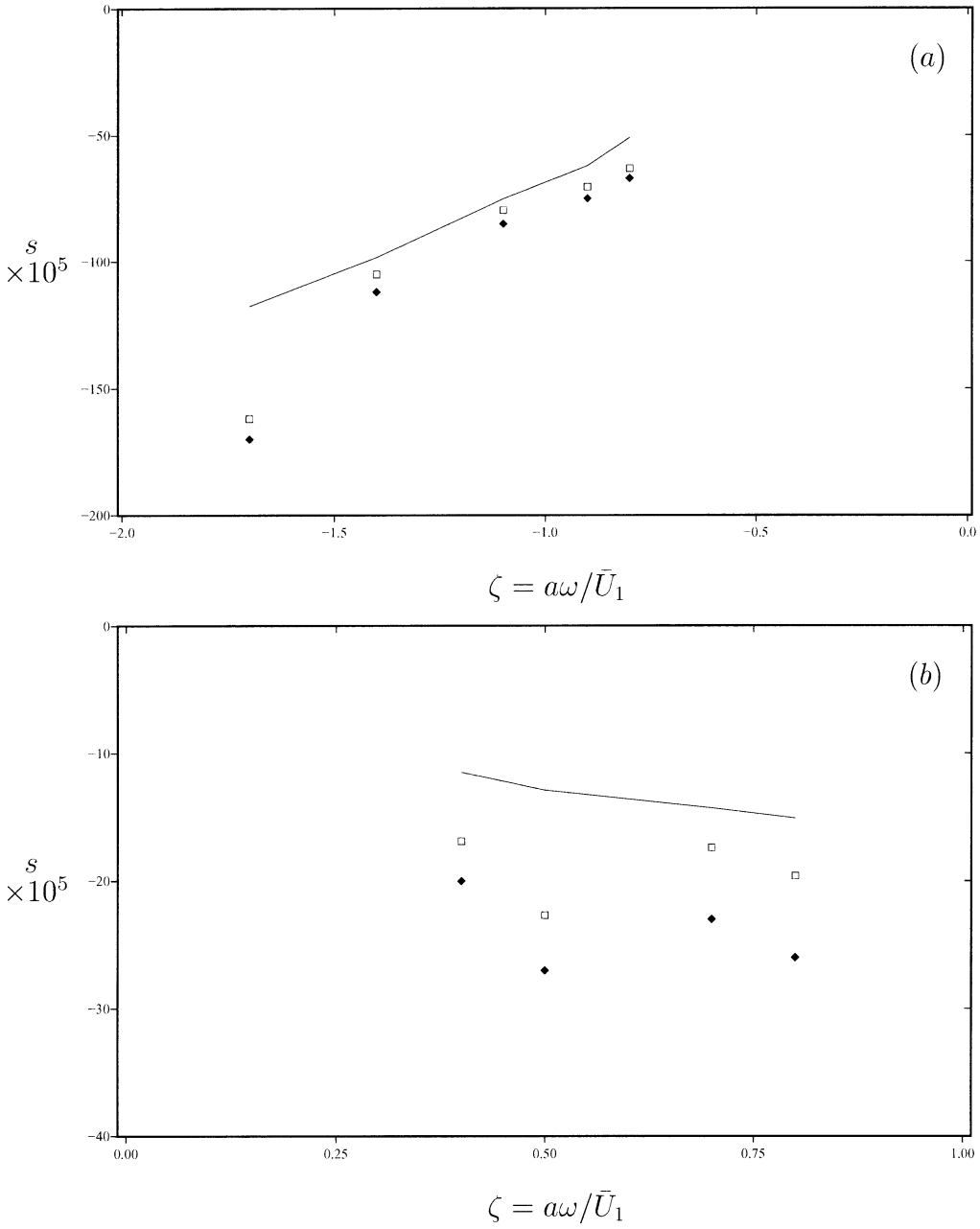

Fig. 3. Wave amplitude decay rates plotted against wave to current strength ratio ζ, Kemp and Simons' data: (a) adverse current; (b) favourable current; ◆ raw experimental data; □ experimental data corrected for side-wall contribution; — computed values.

5.3. Wave decay rates in field conditions

The presence of sidewalls in laboratory wave channels, in addition to scaling effects, raise difficulties when trying to extrapolate laboratory data to field situations. The aim of the present section is to provide benchmark values of wave amplitude decay rates in field conditions. We are not aware of any field measurements of wave decay rates in the presence of well-established steady currents, a further complication of field data being that large areas of constant depth are scarce, which means that it would be quite difficult to distinguish between wave attenuation due to bed friction and wave transformation due to shoaling. Therefore, our computations will not be compared with experimental values.

The field parameters chosen are $D = 10$ m, $T = 8$ s, $a = 1$ m and a bed roughness $z_0 = 0.5$ cm, corresponding to typical swell conditions over a rippled bed on the western Europe continental shelf. Table 3 summarises the depth-averaged currents which have been considered in the adverse and favourable current computations. The currents corresponding to $|\zeta| = 0.25$ are clearly very strong but this has been considered to exemplify the influence of currents on wave damping.

Table 2
Wave amplitude decay rates in the experiments of Mathisen and Madsen (1992)

Experiment ID	Wave-current strength $\zeta = a\omega/\bar{U}_1$	Exp. decay rate (total) $s_e \times 10^5$	Exp. decay rate (sidewall) $s_{es} \times 10^5$	Exp. decay rate (bed) $s_{eb} \times 10^5$	Computed decay rate $s_c \times 10^5$
Rough wall, waves alone					
a	∞	−43.6	−3.3	−40.3	−31.4
b	∞	−39.6	−2.9	−36.7	−27.3
c	∞	−33.5	−2.6	−30.9	−25.2
Rough wall, favourable current					
A	+0.9	−33.9	−3.1	−30.8	−21.4
B	+0.8	−29.6	−2.6	−27.0	−18.6
C	+0.7	−30.0	−2.3	−27.7	−16.6
G	+1.2	−34.6	−3.1	−31.5	−28.6
H	+1.1	−28.9	−2.6	−26.3	−26.2
I	+1.0	−37.4	−2.4	−35.0	−24.1
L	+0.6	−21.8	−1.6	−20.2	−9.1

There is an obvious similarity between modifications of wavelength (or real wave number) and modifications of imaginary wave number in the presence of currents, although this has not been emphasised in the literature to our knowledge. Fig. 5 displays the real part of the wave number, made dimensionless with the flow depth D, plotted against the wave current strength parameter ζ. For comparison purposes the solutions to the dispersive equation

$$(\omega - k_r\bar{U}_1)^2 = gk_r \tanh k_r D, \tag{43}$$

where $\bar{U}_1$ is the depth-averaged current, have been plotted as continuous lines. The roots of Eq. (43) are constrained by $k_r \geq 0$ and $\omega - k_r\bar{U}_1 \geq 0$, which is the solution that exhibits the Doppler shift effect and the appropriate correction for dispersion [9,19]. These correspond to the so-called 'equivalent current' approximation. Also plotted in Fig. 5, and appearing as the horizontal broken line, is the wave number for waves alone which is obtained upon setting $\bar{U}_1 = 0$ in Eq. (43). We find from these different solutions the known result that waves travelling upstream are shorter, and waves travelling downstream longer, than waves with the same absolute period travelling on fluid at rest. The equivalent current approximation is an excellent fit to the real wave numbers output by the model. This result is also in agreement with early findings obtained with inviscid models [27].

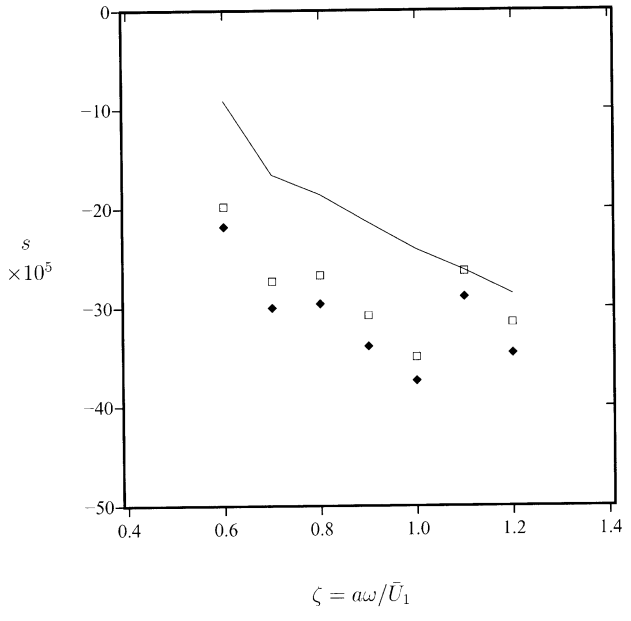

Fig. 4. Wave amplitude decay rates plotted against wave to current strength ratio, ζ, Mathisen and Madsen' data, favourable current; ◆ raw experimental data; □ experimental data corrected for side-wall contribution; — computed values.

Fig. 6 pictures the dimensionless imaginary wave numbers k_i corresponding to Fig. 5. We recall that k_i governs the wave amplitude decay rate as shown in Eq. (2). Once again, the horizontal broken line is the solution for waves propagating on fluid at rest. The same qualitative behaviour as reported in the Kemp and Simons' experiments are here observed. Waves travelling downstream have smaller damping rates than waves alone; waves travelling upstream have significantly higher damping rates. The vertical asymptotic branch of the adverse current curve, when $|\zeta| \to 0$, corresponds to another known result that surface waves cannot travel on an opposing current faster than their group velocity.

For practical purposes damping rates can be derived by simple reading of Fig. 6. For instance, the present model predicts a 8s-wave meeting the opposing current with $\zeta = -1.5$ (i.e. $\bar{U}_1 = -0.52$ m/s, see Table 3) would loose 99% of its initial amplitude in 24 km. Conversely, the same wave

Table 3
Values of the wave current strength parameter $\zeta = a\omega/\bar{U}_1$ considered in the field condition computations. The flow depth is $D = 10$ m and the wave parameters are $T = 8$ s, $a = 1$ m

$\lvert\zeta\rvert$	0.25	0.5	1.0	1.5	2.0	4.0
$\lvert\bar{U}_1\rvert$ (m/s)	3.14	1.57	0.78	0.52	0.39	0.20

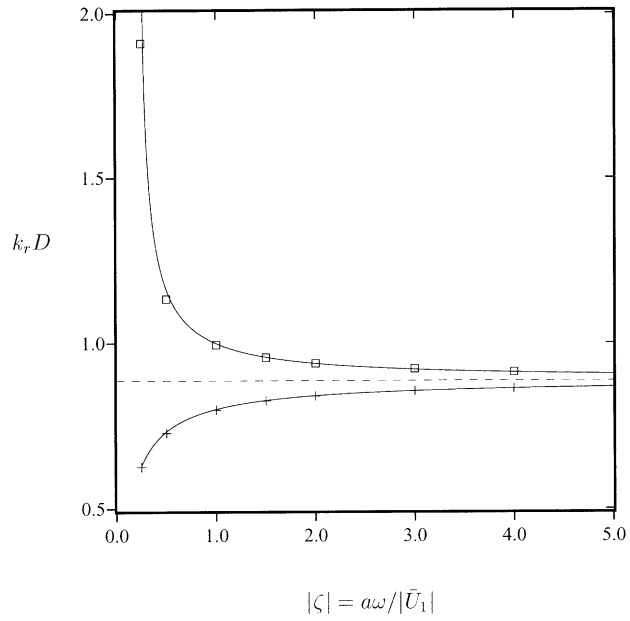

Fig. 5. Dimensionless real-part of the wave number in field conditions, $D = 10$ m, $T = 8$ s, $a = 1$ m, plotted against absolute value of the relative wave to current strength parameter ζ. +, present study, Following current; □, present study, adverse current. —, uniform current approximation; - - -, waves alone (no current).

propagating downstream on a current with the same magnitude would need 64 km to loose the same fraction of its initial amplitude. Such currents are commonly encountered in tide-dominated environments. The increase in damping rate is much more dramatic for the strongest

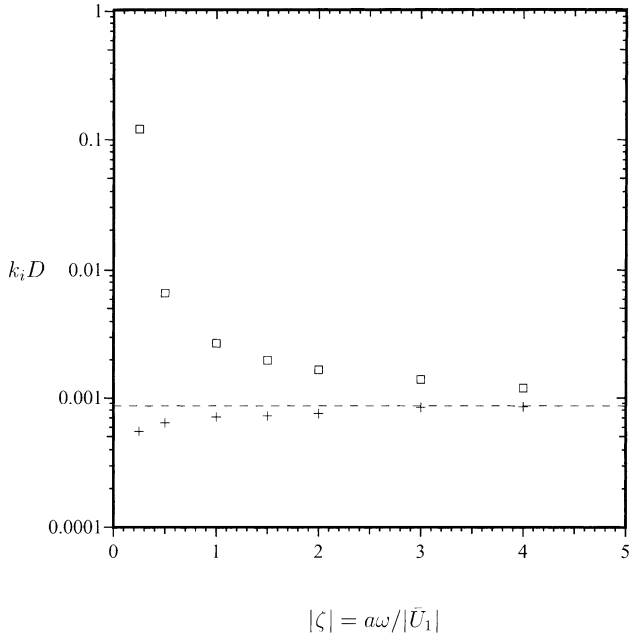

Fig. 6. Dimensionless imaginary wave number in field conditions, $D = 10$ m, $T = 8$ s, $a = 1$ m (same data as Fig. 5), plotted against absolute value of the relative wave to current strength parameter ζ. +, Following current; □, adverse current; - - -, waves alone (no current).

opposing current in Fig. 6. This flow corresponds to a very high current magnitude ($\bar{U}_1 = -3.14$ m/s, Table 3) which can be occasionally observed during equinoctial tides in the English Channel for instance, or at the mouth of some river outlets. In that particular case the magnitude of $\bar{U}_1$ is approximately half the group velocity of the wave train. The present model predicts a 8s-wave meeting this very strong opposing current would loose 99% of its initial amplitude in 400 m; in clear it would be blocked by the current in a few wavelengths. Conversely, the same wave travelling downstream would need 84 km to be damped in the same proportion.

When extrapolating from Fig. 6 it should be born in mind that the sole effect of bed friction has been incorporated, shoaling effects and wave attenuation due to percolation are not taken into consideration.

6. Discussion and conclusion

A model has been presented that solves the full-depth flow of free surface waves in the presence of collinear turbulent currents. Currents, which must be input to the present model, have been here computed in the first place with a numerical boundary layer wave current model [25]. The results have been focused on the prediction of the wave number, the real part of it accounting for wavelength modifications in the presence of currents, the imaginary part accounting for wave damping. We have presented different comparisons between laboratory data and model predictions. Our computations confirm the findings of Kemp and Simons, i.e. waves propagating downstream are less damped, and waves propagating upstream significantly more damped, than waves on fluid at rest. This result has been tested against laboratory data and appears to hold in field conditions (Fig. 6), although here no field data were used to confirm the hypothesis. It can probably be interpreted in terms of an energy balance between the waves and the current. In a boundary layer approximation, one can show [16] that the wave friction factor is inversely proportional to $c_g + \bar{U}_1$ (c_g = wave group velocity, $\bar{U}_1$ = depth − averaged current). On a following current, the friction factor should decrease with increasing current magnitude; for an adverse current the friction factor should increase with increasing current magnitude, until the waves get clamped when $\bar{U}_1 \simeq -c_g$. The results of the present model (see for instance Fig. 6), together with the laboratory experimental evidence, are consistent with this interpretation.

Looking more carefully into the details of the results for the mean wave decay rates, one can say that there is good to excellent agreement for the adverse current experiments of Kemp and Simons (see Fig. 3a). For waves propagating with a following current our model systematically under-predicts the decay rates measured by Kemp and Simons and Mathisen and Madsen. The discrepancy between predicted and computed wave decay rates can be as high as 50% for

both data sets; see Figs. 3b and 4 and the corresponding tables. There is an apparent tendency of the model to give better results at higher values of the wave current strength parameter ζ.

When trying to interpret these favourable current results one should consider the following points:

- The model results for the waves alone decay rates are also under-predicting the experimental values, this being more pronounced with the Mathisen and Madsen's data. It would be possible to improve this behaviour by tuning some of the model constants of the turbulence closure, but our choice was to keep strictly the same model as originally derived by Chien [3].
- Although ζ is in the same range in both data sets the relative reduction in the wave current decay rates, with respect to the waves alone decay rates, is clearly more pronounced in the Kemp and Simons' experiments.
- Experiments labelled J and K in Mathisen and Madsen's paper have markedly smaller wave decay rates, although their ζ is the same as in experiments B and C, respectively. The model results for experiments J and K (not shown in Fig. 4 to avoid confusion) are not better than those of experiments B and C.

It seems rather difficult to imagine a model that could explain, and (or) correct, all these features. The different roughness elements used and the different aspect ratios of the wave tanks are possible explanations, although this remains pure speculation. These remarks demand more laboratory experiments, and surely model developments.

Whether the present model can be used as it stands now as a predictive tool is still open to discussion since validation against data has not been fully satisfactory in different experimental conditions. This model, appearing as a first step towards trying to reconcile boundary layer and full-depth inviscid models, bears many potential improvements. The first obvious phenomenon that has been ignored is the mean depth setup [21]. However, one should be aware that Sato found the mean surface setup to contribute a positive attenuation rate, which means the predicted decay rates for favourable currents taking this effect into account would be even farther from the experimental values considered. In the meantime this author pointed out that bed friction is the main cause of wave damping in most practical situations. Finally, there should be no more than technical difficulties in extending the present formulation to regular waves propagating at an angle with the mean current. The extension to random waves seems in contrast a rather difficult challenge.

Acknowledgements

This work was undertaken as part of the MAST project The Kinematics and Dynamics of Wave-Current Interactions. It was funded by the Commission of the European Union Directorate General for Science, Research and Development under contract no. MAS3-CT95-0011. Support is also acknowledged from the research project Dynamique du système côtier du Pas-de-calais (DYSCOP) funded by the Nord-Pas de Calais regional council under contracts no. DYSCOP-USTL-2641/9384 and 907/F001.

References

[1] Brevik I, Aas B. Flume experiments on waves and currents I. Rippled bed. Coastal Engng 1980;3:149–77.
[2] Celik I, Rodi W. Simulation of free-surface effects in turbulent channel flows. Phys Chem Hydr 1984;5(3):217–27.
[3] Chien KY. Predictions of channel and boundary layer flows with a low-Reynolds-number turbulence model. AIAA J 1982;20:33–8.
[4] Davies AG, Soulsby RL, King HL. A numerical model of the combined wave and current bottom boundary layer. J Geophys Res 1988;93(C1):491–508.
[5] Fenton JD. Some results for surface gravity waves on shear flows. J Inst Math Applic 1973;12:1–20.
[6] Groeneweg J, Klopman G. Changes of the mean velocity profiles in the combined wave current motion described in a GLM formulation. J Fluid Mech 1998;370:271–96.
[7] Hunt JN. Viscous damping of waves. La Houille Blanche 1952;7:836–42.
[8] Jonsson IG. Wave-current interactions. In: Le Méhauté B, Hanes DM, editors. The sea (Ocean Engng Sci), vol. 9(A). New York: Wiley, 1990. p. 65–120.
[9] Jonsson IG, Skougaard C, Wang JD. Interaction between waves and currents. Proceedings of the 12th Coastal Engineering Conference, ASCE, 1970. p. 489–508.
[10] Kemp PH, Simons RR. The interaction between waves and a turbulent current: waves propagating with the current. J Fluid Mech 1982;116:227–50.
[11] Kemp PH, Simons RR. The interaction of waves and a turbulent current: waves propagating against the current. J Fluid Mech 1983;130:73–89.
[12] Klopman G. Vertical structure of the flow due to waves and currents. Technical Report H840.30, Part 1, Delft Hydraulics, Delft. 1992, 57p.
[13] Klopman G. Vertical structure of the flow due to waves and currents. Technical Report H840.30, Part 2, Delft Hydraulics, Delft. 1994, 39p.
[14] Klopman G, Madden N, Thais L, Groeneweg J, Simons RR. An intercomparison study of complete oscillatory flow models for wave current interaction, in preparation.
[15] Madden N, Stynes M, Thomas GP. On the development of complete flow models for wave current interactions. Proceedings of the Coastal Dynamics Conference, ASCE, Plymouth, UK, 1997. p. 105–41.
[16] Massel SR. Hydrodynamics of coastal zones, Elsevier oceanography series, vol. 48, 1989. 336p.
[17] Mathisen P, Madsen OS. Waves and currents over a fixed rippled bed 1. Bottom roughness experienced by waves in the presence and absence of currents. J Geophys Res 1996;101(C7):16,533–42.
[18] Nielsen P. Coastal bottom boundary layers and sediment transport, Adv Ser Ocean Engng. Singapore: World Scientific, 1992. 323p.
[19] Peregrine DH. Interaction of water waves and currents. Adv Appl Mech 1976;16:9–117.
[20] Reynolds WC, Hussain AKMF. The mechanics of an organized wave in turbulent shear flow 3. Theoretical model and comparisons with experiments. J Fluid Mech 1972;54:263–88.
[21] Sato M. On the attenuation of waves propagating with a current.

Proceedings of the 23rd Coastal Engineering Conference, ASCE, 1992. p. 563–75.

[22] Simons RR, Grass AJ, Kyriacou A. The influence of currents on wave attenuation. Proceedings of the 21st Coastal Engineering Conference, ASCE, 1988. p. 363–76.

[23] Soulsby RL, Hamm L, Klopman G, Myrhaug D, Simons RR, Thomas GP. Wave-current interaction within and outside the bottom boundary layer. Coastal Engng 1993;21:41–69.

[24] Thais L, Chapalain G, Smaoui H. Reynolds number variation in oscillatory boundary layers Part I: purely oscillatory motion. Coastal Engng 1999;36:111–46.

[25] Thais L, Chapalain G. Reynolds number variation in oscillatory boundary layers. Part II: Wave-current interactions. MAST Report (Kinematics and Dynamics of Wave-Current Interactions), Appendix-III, 1999. 23p.

[26] Thais L, Magnaudet J. Turbulent structure beneath surface gravity waves sheared by the wind. J Fluid Mech 1996;328:313–44.

[27] Thomas GP. Wave-current interactions: an experimental and numerical study Part 1. Linear waves. J Fluid Mech 1981;110:457–74.

[28] Thomas GP, Klopman G. Wave-current interactions in the near-shore region. Adv Fluid Mech (Gravity waves in water of finite depth) 1997;6:257–322.

[29] Yih CS. Surface waves in flowing water. J Fluid Mech 1972;51:209–20.